Acta Materialia 107 (2016) 144–151

Contents lists available at ScienceDirect

Acta Materialia

journal homepage: www.elsevier.com/locate/actamat

Full length article

Multiscale modeling of hydrogen enhanced homogeneous dislocation nucleation

G.P.M. Leyson*, Blazej Grabowski, Jörg Neugebauer

Max-Planck-Institut für Eisenforschung GmbH, Düsseldorf 40237, Germany

ARTICLE INFO

Article history:
Received 22 September 2015
Received in revised form
14 January 2016
Accepted 17 January 2016
Available online 5 February 2016

Keywords:
Homogenous dislocation nucleation
Nanoindentation
Hydrogenhydrogen interaction
Dislocations

ABSTRACT

A multiscale approach is proposed to predict how the presence of hydrogen influences the onset of homogeneous dislocation nucleation (HDN) and thus of plasticity. The model takes inputs that can be solely obtained from atomistic calculations, such as dislocation core structure, stacking fault energy and hydrogen–hydrogen interaction. The equilibrium hydrogen concentration around the dislocation loop is calculated using a recently developed self-consistent iterative method [1]. The complex nature of the dislocation field, as well as the equilibrium hydrogen concentration around the loops, is taken into account. The onset of HDN as a function of bulk hydrogen concentration and temperature is quantitatively predicted and is consistent with nano-indentation experiments on hydrogen loaded samples. Applying the approach to Ni, we find that even low hydrogen concentrations of about 1 at-% result in largely reduced HDN energy barriers and thus largely reduce the critical shear stress.

1. Introduction

Hydrogen embrittlement is a century-old problem [2] that is known to occur in a wide range of materials [3–14]. This phenomenon is particularly severe in ferritic high strength steels due to the high mobility of hydrogen solutes in bcc iron. However, despite the growing interest in the topic, the underlying mechanisms that cause hydrogen embrittlement are not well-understood. The difficulty is rooted in the different time- and length-scales associated with the phenomenon. Hydrogen diffusion at relevant temperatures is fast relative to experimental time-scales, but not fast enough to be easily simulated using current computational technology. On the other hand, both atomic and mesoscopic length-scales are relevant due to nontrivial solute–solute interactions and defects such as dislocations and cracks with long-range elastic fields.

Several conceptual frameworks have been proposed to explain hydrogen embrittlement, including hydride formation and cleavage [10,15], hydrogen enhanced decohesion (HEDE) [5–7,13,16–18], and hydrogen enhanced local plasticity (HELP) [3,4,8,11,12,19–24]. In particular, the HELP mechanism is based on the localization of hydrogen around dislocations. Once this happens, it is thought that the hydrogen modifies the interaction of dislocations with other defects (such as other dislocations) and results in local plasticity that is macroscopically similar in fracture appearance to brittle fracture. While various aspects of this mechanism have been extensively studied, a quantitative connection between the hydrogen localization around dislocations and the actual brittle-like macroscopic behavior has yet to be made. In order to make this connection, the interaction between the hydrogen solutes and dislocations must be accurately quantified and understood.

A powerful experimental methodology to study this interaction is through *in situ* electrochemical nanoindentation experiments charged with hydrogen [25]. In these experiments, homogeneous dislocation nucleation (HDN) in hydrogen-charged metal samples is initiated by a nanoindenter. These experiments have the advantage of having a well-defined system that facilitates the comparison between experiments and theory. Due to the small sampling volume, grain boundaries and other hard-to-characterize and describe defects (i.e. forest dislocations) do not affect the results, and one can reasonably assume that the region at which the nucleation occurs locally resembles a perfect crystal. The system also circumvents the common problem when describing the energy of systems containing dislocations. A straight dislocation has a long-range stress field which scales like $1/r$. This means that, in principle, the interaction with solutes very far away from the dislocation cannot be ignored. Dislocation loops, however, do not have a long-range field and only solutes close to the dislocation are relevant in

* Corresponding author. Max-Planck-Straße 1, 40237 Düsseldorf Germany.
E-mail address: g.leyson@mpie.de (G.P.M. Leyson).

http://dx.doi.org/10.1016/j.actamat.2016.01.036
1359-6454/

the analysis. Finally, analytic solutions to the stress field underneath the indenter prior to dislocation nucleation are well-defined [2].

The effect of hydrogen on nanoindentation experiments has been attributed to changes in the shear modulus, dislocation core structure and/or stacking fault energy due to hydrogen [25,26]. These changes were treated as fitting parameters for the experimental data and the localization of hydrogen around the dislocation was not explicitly taken into account. More recently, Kirchheim [27] proposed a thermodynamic framework wherein hydrogen acts to lower the dislocation line energy through favorable interaction with the dislocation. To quantitatively evaluate this effect, one has to know how much hydrogen is localized around the dislocation loops as well as determine the strength of the interactions. Apart from the solute-dislocation interaction, hydrogen–hydrogen interaction also plays a crucial role and may even lead to the formation and stabilization of hydrides around dislocations [1,28].

In this paper, we derive and employ a multiscale approach that allows us to describe the full complexity of forming and stabilizing a dislocation loop both in the absence and presence of hydrogen. Specifically, we develop an analytic model that is informed by atomistic inputs, such as hydrogen–hydrogen interaction and the geometry of the dislocation core, and takes into account the discrete nature of the system. The model calculates the equilibrium hydrogen concentration around a dislocation at finite temperature and quantitatively predicts the onset of HDN as function of applied shear stress.

2. Computational methods

A schematic representation of our simulation box is shown in Fig. 1. An orthagonal supercell is created with principal directions corresponding to the $[\bar{1}10](111)$ slip system. The size of the simulation box is 63.5 Å × 72.1 Å × 63.9 Å, containing 28080 Ni atoms. The size of the simulation box was chosen such that the elastic energy of the largest dislocation loop considered is converged with respect to system size to within 0.1%. Faulted hexagonal loops with partial Burgers vector $\boldsymbol{b}^p = a_{\mathrm{Ni}}/6[\bar{1}2\bar{1}]$ are considered, where a_{Ni} is the lattice parameter of Ni. This is because, at small loop radii that are relevant to nucleation, faulted hexagonal loops are energetically more favorable than full dislocation loops in *fcc* metals [29]. Hydrogen atoms are assumed to occupy only the octahedral sites in the system.

The energetics of the system is described using an analytic model that takes key inputs from atomistic calculations, such as local hydrogen–hydrogen interaction and dislocation core structure. In the analytic model, the system is assumed to be an isotropic linear elastic material. The hydrogen solutes are approximated as point dilatational sources. Since the most important interaction in the system is that of the hydrogen solutes and the stress fields, the elastic constants chosen are the bulk modulus K and the Poisson ratio ν in the coordinate system above.

The atomistic calculations were performed using a modified semi-empirical embedded atom method (EAM) potential based on a potential developed by Angelo et al. [30]. The modification of the original potential was done in Ref. [28] by increasing the cut-off radius r_{cut} of the Ni–H interaction from 4.83 Å to 4.92 Å in order to remove elastic instabilities arising from a negative C_{44} of the rocksalt Ni–H structure without affecting other relevant properties of the system. The materials properties that are obtained using this potential are summarized in Table 1.

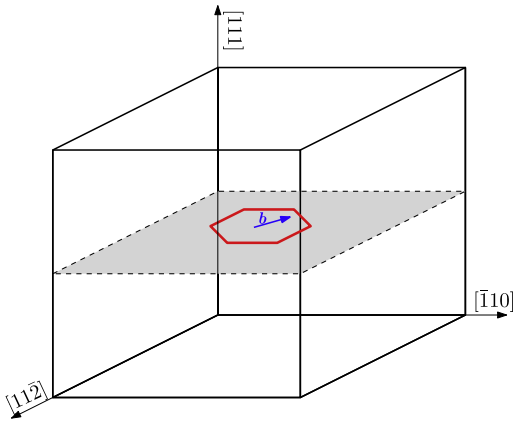

Fig. 1. A schematic representation of the simulation cell used to model Homogeneous Dislocation Nucleation (HDN). A faulted hexagonal dislocation loop (solid red line) with Burgers vector $\boldsymbol{b}^p = a_{\mathrm{Ni}}/6[\bar{1}2\bar{1}]$ is introduced to the system. (For interpretation of the references to colour in this figure legend, the reader is referred to the web version of this article.)

3. Energetics

To determine when the homogeneous dislocation nucleation can spontaneously occur, the free energy of the system at finite temperature must be considered. Consider a system coupled to a hydrogen reservoir with chemical potential μ_{H}. The temperature T along with μ_{H} determines the equilibrium bulk hydrogen concentration $c_{\mathrm{H}}^{\mathrm{bulk}}$. We define the bulk hydrogen concentration as the ratio between the actual number of hydrogen atoms in the defect free, unstressed bulk and the maximum number of available bulk interstitial sites they can be incorporated. The latter number is identical to the number of Ni atoms. When the bulk hydrogen concentration $c_{\mathrm{H}}^{\mathrm{bulk}} \ll 1$, the free energy f° per host atom is,

$$f^{\circ} = e_{\mathrm{Ni}} + c_{\mathrm{H}}^{\mathrm{bulk}}\left[(e_{\mathrm{H}} - \mu_{\mathrm{H}}) + kT \ln c_{\mathrm{H}}^{\mathrm{bulk}}\right], \tag{1}$$

where e_{Ni} is the energy of pure fcc Ni per atom, e_{H} is the energy of inserting one H atom in the Ni matrix in the dilute limit. Hydrogen–hydrogen interaction is assumed to be negligible in Eq. (1), since $c_{\mathrm{H}}^{\mathrm{bulk}}$ is small in typical experimental conditions. It should be emphasized that $c_{\mathrm{H}}^{\mathrm{bulk}}$ refers specifically to the concentration of hydrogen in the unstressed bulk. The local concentration of hydrogen can be significantly higher in regions with large tensile stresses. The term e_{H} is determined by molecular static calculations using 5 × 5 × 5 conventional supercells,

$$e_{\mathrm{H}} = E_{\mathrm{tot}}^{1H} - E_{\mathrm{tot}}^{\mathrm{bulk}}, \tag{2}$$

where $E_{\mathrm{tot}}^{1\mathrm{H}}$ is the energy of the supercell containing one H atom and $E_{\mathrm{tot}}^{\mathrm{bulk}}$ is the total energy of the supercell without any H atoms. The equilibrium bulk hydrogen concentration can be determined by minimizing Eq. (1) with respect to $c_{\mathrm{H}}^{\mathrm{bulk}}$,

$$c_{\mathrm{H}}^{\mathrm{bulk}} = \exp\left(-\frac{e_{\mathrm{H}} - \mu_{\mathrm{H}}}{kT}\right). \tag{3}$$

When a dislocation loop is introduced in the system, the stress gradient induced by the loop changes the local hydrogen concentration around the loop. The change in free energy with respect to the perfect bulk is,

$$\Delta F^{\mathrm{loop}} = \sum_{i}^{N_{\mathrm{oct}}}\left(\Delta f_i^{\mathrm{f}} + \Delta f_i^{\mathrm{lb}} + \Delta f_i^{\mathrm{S}}\right) + \Delta F^{\mathrm{disl}}, \tag{4}$$

where

Table 1
Elastic constants, stable stacking fault energy γ_{sf} and misfit volume Δv_m as given by the modified EAM potential, DFT [28], and experiments [30] for pure Ni and rocksalt NiH.

	C_{11} (GPa)	C_{12} (GPa)	C_{44} (GPa)	K (GPa)	γ_{sf} (mJ/m^2)	Δv_m (Å^3)
Pure fcc Ni						
EAM [28]	251.1	144.1	133.9	179.8	162	3.5
DFT [28]	267.5	153.6	129.3	191.6	–	2.3
Experiment [30]	246.4	147.3	124.7	180.3	125	3.2
Rocksalt NiH						
EAM [28]	281.5	186.2	32.4	217.9	–	–
DFT [28]	281	169	77	207.1	–	–

$$\Delta f_i^{\mathrm{f}} = \left(c_{\mathrm{H}}^i - c_{\mathrm{H}}^{\mathrm{bulk}}\right)(e_{\mathrm{H}} - \mu_{\mathrm{H}}) \tag{5}$$

is the change in formation energy due to the change in local hydrogen concentration at octahedral site i,

$$\Delta f_i^{\mathrm{lb}} = c_{\mathrm{H}}^i \Delta u_b^i \tag{6}$$

is the change due to the local change in hydrogen binding energy Δu_b^i arising from the interaction of the H atoms with the dislocation stress field, as well as additional H–H interaction from increased concentration of neighboring sites. Further in Eq. (4),

$$\Delta f_i^{\mathrm{S}} = kT\left[c_{\mathrm{H}}^i \ln c_{\mathrm{H}}^i + \left(1 - c_{\mathrm{H}}^i\right)\ln\left(1 - c_{\mathrm{H}}^i\right) - c_{\mathrm{H}}^{\mathrm{bulk}} \ln c_{\mathrm{H}}^{\mathrm{bulk}}\right] \tag{7}$$

is the change in entropy of the system due to local changes in hydrogen concentration. Finally, ΔF^{disl} is the increase in free energy due to the dislocation loop and is determined by calculating the stress $\sigma_{ij}^{\mathrm{disl}}$ and strain $\varepsilon_{ij}^{\mathrm{disl}}$ fields at each Ni site, and considering the additional energy due to the introduction of the stacking fault within the dislocation loop,

$$\Delta F^{\mathrm{disl}} = \sum_k^{N_{\mathrm{Ni}}} \frac{1}{2}\sigma_{ij}^{\mathrm{disl}}(r_k)\varepsilon_{ij}^{\mathrm{disl}}(r_k)v_{\mathrm{Ni}} + \gamma_{\mathrm{sf}}A_{\mathrm{disl}},$$

where v_{Ni} is the volume of a Ni atom, γ_{sf} is the stable stacking fault energy of Ni and A_{disl} is the area of the dislocation loop. The entropy change due to the dislocation loop is ignored as it is much smaller compared to the entropy of the H solutes.

The stress field $\sigma_{ij}^{\mathrm{ind}}$ due to the indenter changes the free energy of the system further. The change in free energy $\Delta F^{\mathrm{loop+ext}}$ from a perfect crystal under the indenter to a crystal containing a dislocation loop under the indenter is given by

$$\Delta F^{\mathrm{loop+ext}} = \Delta F^{\mathrm{loop}} + \Delta F^{\mathrm{ext-loop}} + \Delta F^{\mathrm{ext-H}} \tag{8}$$

where $\Delta F^{\mathrm{ext-loop}}$ is the interaction energy of the dislocation with the indenter and $\Delta F^{\mathrm{ext-H}}$ is the interaction of the indenter with the H solutes. The term $\Delta F^{\mathrm{ext-loop}}$ is equivalent to the work done by the dislocation loop in the presence of the external field and is given by

$$\Delta F^{\mathrm{ext-loop}} = \tau b^p A \tag{9}$$

where b^p is the magnitude of the partial Burgers vector of the dislocation loop, τ is the shear stress in the direction of the Burgers vector and A is the area inside the loop. The term $\Delta F^{\mathrm{ext-H}}$ only depends on the pressure field of the indenter and results in an effective decrease in the bulk hydrogen concentration under the indenter.

4. Stress field of a faulted hexagonal dislocation loop

The stress, strain and displacement fields of a faulted hexagonal loop [31,32] are calculated using discrete Volterra segments. The equations used for this calculation are summarized in Appendix A. The elastic fields of regular hexagonal Volterra loops were calculated from $r^{\mathrm{disl}} = 0$ to $r^{\mathrm{disl}} = 10b$ at $0.1b$ intervals, where $b = a_{\mathrm{Ni}}/\sqrt{2}$ is the full Burgers vector of the system. In fcc materials and other close-packed systems, dislocations are delocalized within the slip plane [33]. Volterra loops are therefore insufficient in describing the elastic fields close to the dislocation loops. A good description for such dislocations is the Peierls-Nabarro model, which takes into account the atomic displacements due to the dislocation in the slip plane. In this work, we approximate the Peierls-Nabarro model by superimposing the elastic fields of Volterra loops with the appropriate weights.

The stress field of a Peierls-Nabarro (PN) loop with radius r^{disl} is then given by

$$\sigma_{ij}^{\mathrm{PN}}\left(r^{\mathrm{disl}}\right) = \sum_i w\left(r_i, r^{\mathrm{disl}}\right)\sigma_{ij}^V(r_i) \tag{10}$$

where $\sigma_{ij}^V(r_i)$ is the stress field of a Volterra loop with radius r_i and $w(r_i,r^{\mathrm{disl}})$ is the weight of that loop. The corresponding strain tensor can be calculated using the compliance tensor of Ni (i.e., $\varepsilon_{ij}^{\mathrm{PN}} = S_{ijkl}\sigma_{kl}^{\mathrm{PN}}$).

The weight is obtained by assuming an arctangent distribution of the Burgers vector along the slip plane,

$$w\left(r_i, r^{\mathrm{disl}}\right) = \frac{1}{\pi\Lambda}\left[\frac{1}{1 + \left(\frac{r_i - r^{\mathrm{disl}}}{\Lambda}\right)^2} - \frac{1}{1 + \left(\frac{r_i + r^{\mathrm{disl}}}{\Lambda}\right)^2}\right]\Delta x, \tag{11}$$

where Λ is the characteristic partial spreading of the dislocation partial and $\Delta x = 0.1b$ is the spacing of the Volterra solutions. The term Λ is determined to be 3 Å from our previous work on straight Ni edge dislocations [1], and is obtained by matching the Nye tensor of the dislocation core obtained from our analytic model to that of the core obtained from direct molecular static calculations. The first term in Eq. (11) corresponds to the Burgers vector distribution of the segment along the slip plane, while the second term corresponds to that of the segment directly opposite to the segment located $2r^{\mathrm{disl}}$ away. This contribution has a negative sign due to the fact that the opposite segment always has the opposite line sense. The weight distribution $w(r^i,r^{\mathrm{disl}})$ ensures a smooth elastic energy profile from a perfect crystal to one containing a full faulted dislocation loop. Fig. 2 shows the displaced Ni position of a PN loop with $r^{\mathrm{disl}} = 4b$, revealing a stacking fault inside the dislocation loop, as expected.

The elastic fields in this description are not accurate on sites close the dislocation core region. This is because the stacking fault

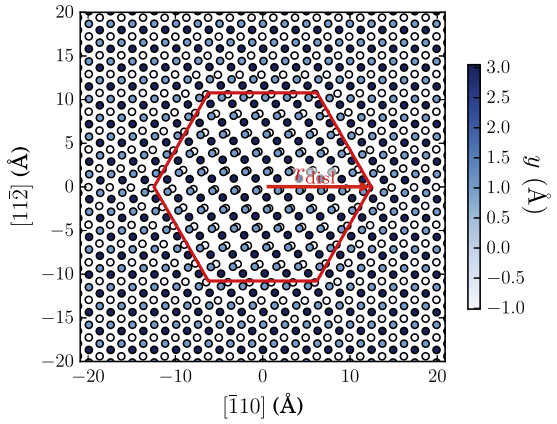

Fig. 2. The displaced Ni positions of a crystal containing a faulted, hexagonal PN loop with $r^{disl} = 4b$. Three atomic layers are shown, with the colors corresponding to the out of plane coordinate of the Ni sites. Outside the dislocation loop *ABC*-stacking is observed, indicating a near-perfect fcc structure. Inside the dislocation, the white Ni atoms eclipse the dark blue atoms, indicating a local *ABA*-stacking.

energy in the immediate vicinity of the partials is significantly higher than the stable stacking fault energy. Because of this, the elastic energy of small dislocation loops on the order of the partial spreading Λ is expected to be underestimated. Note that this is analogous to a classical analysis wherein results are expected to be inaccurate when the loop radius is on the order of the core cut-off radius [33].

5. Local hydrogen concentration and binding energy

The binding energy of the dislocation arises from the interaction between the H solutes and the dislocation stress field. Traditionally, only this elastic interaction has been considered, though recent works [28,34] have shown that H–H interaction plays an important role. Taking H–H interaction into account leads to hydrogen localization around stress concentrators and may cause the formation of local (nano) hydrides. This contribution can therefore not be neglected. The hydrogen binding energy Δu_b^i at octahedral site i is therefore assumed to be composed of two components; the elastic interaction between the dislocation Δu_{el} and the H–H interaction Δu_{H-H} [1],

$$\Delta u_b^i(\boldsymbol{r}_i, c_H) = \Delta u_{el}^i(\boldsymbol{r}_i) + \Delta u_{H-H}^i(\boldsymbol{r}_i, c_H). \tag{12}$$

Since the H solutes are considered as point dilational sources, the elastic interaction only involves the pressure fields of the dislocation and the indenter, p^{disl} and p^{ind}. More specifically,

$$\Delta u_{el}^i(\boldsymbol{r}_i) = -\left(p^{disl}(\boldsymbol{r}_i) + p^{ind}(\boldsymbol{r}_i)\right)\Delta v_m, \tag{13}$$

where $\Delta v_m = 3.5$ Å^3 is the misfit volume of H in Ni.

The binding due to H–H interaction Δu_{H-H} is taken to be a quadratic function of 1^{st} and 2^{nd} nearest neighbors of the octahedral site,

$$\Delta u_{H-H}^i(\boldsymbol{r}_i, c_H) = A_1\overline{N}_1 + A_2\overline{N}_2 + A_3\overline{N}_1^2 + A_4\overline{N}_2^2 + A_5\overline{N}_1\overline{N}_2, \tag{14}$$

where

$$\overline{N}_1 = \sum_m^{12} c_H(\boldsymbol{r}_m) \tag{15}$$

and

$$\overline{N}_2 = \sum_n^{6} c_H(\boldsymbol{r}_n) \tag{16}$$

is the average number of hydrogen in the 1^{st} and 2^{nd} nearest neighbor sites of octahedral site i located at $\boldsymbol{r}_m$ and $\boldsymbol{r}_n$, respectively. $A_1 = -28.9$ meV, $A_2 = -6.2$ meV, $A_3 = 0.54$ meV, $A_4 = 3.7 \times 10^{-2}$ meV and $A_5 = 0.36$ meV are constants fitted to direct molecular static calculations [1]. The H–H interaction is assumed to be independent of local strain, which is validated by the good agreement of local hydrogen concentration between the model and atomistic/Monte Carlo coupled calculations [1].

Once Δu_b^i is determined, the equilibrium hydrogen concentration on the octahedral site i can be determined by the Fermi-Dirac distribution,

$$c_H\left(\Delta u_b^i, T\right) = \frac{1}{1 + \left(c_H^{bulk}\right)^{-1}\exp\left[\Delta u_b^i / kT\right]}. \tag{17}$$

Due to Δu_{H-H}, the binding energy is a function of the local hydrogen concentration c_H, which in turn is a function of the binding energy. Therefore, Eqs. (12) and (17) must be solved self-consistently in order to fully determine the equilibrium hydrogen concentration profile in the system. This is accomplished by adopting an iterative scheme similar to the one implemented for straight edge dislocation [1]. The scheme goes as follows. The stress field of the dislocation loop σ_{ij}^{disl} is determined by the steps outlined in sec. 4. The elastic binding energy Δu_{el} is then calculated using Eq. (13), which is used to generate the initial hydrogen seed in the system. All sites with $\Delta u_{el}^i < -40$ meV are initially filled with hydrogen (i.e., $c_H^i = 1$). This initial hydrogen concentration profile is used to calculate the total hydrogen binding energy. Using Eq. (17), a new concentration profile is calculated and compared to the previous c_H. These steps are iterated until the maximum error between the old c_H^i and the new c_H^i is less then 0.1%. Calculating a converged hydrogen concentration profile using this method is highly computationally efficient and takes on the order of minutes to accomplish.

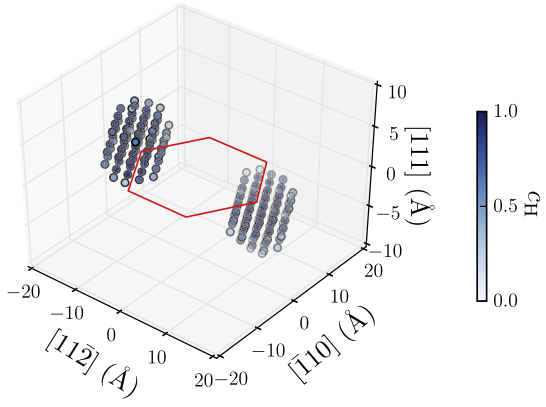

Fig. 3. The equilibrium concentration profile c_H of hydrogen for a dislocation loop with $r^{disl} = 4b$ and $c_H^{bulk} = 1000$ ppm. For clarity, only sites with $c_H^i > 0.3$ are shown in the figure. Local hydride formation can be observed in the regions with large tensile pressure fields.

6. Results and discussion

6.1. Energetics of dislocation loops under pure shear load

Let us first examine the energetics of the system for the case when an external shear stress τ^{ext} is applied in the direction of the partial Burgers vector $\boldsymbol{b}^p$. In this case, the hydrostatic component of the external field is zero (i.e., $\sigma_{kk}^{\text{ext}} = 0$). A typical concentration profile is shown in Fig. 3 for $r^{\text{disl}} = 4b$, $c_{\text{H}}^{\text{bulk}} = 1000$ ppm and $T = 300$ K. In the presence of a dislocation loop, the hydrides are observed to decorate regions with high dilatational stress, i.e., segments that have predominantly edge character. Since the hydrogen mainly interacts with hydrostatic stress fields, the elastic interaction energy is most favorable in the tensile regions of the dislocation loop, which leads to an increase in local hydrogen concentration. This increase in local hydrogen concentration is positively reinforced by the hydrogen–hydrogen interaction due to the presence of neighboring hydrogen atoms. This positive reinforcement leads to H concentrations at these segments that are several orders of magnitude larger than the bulk concentration or the concentrations one would find in the absence of an attractive H–H interaction. The resulting hydrogen concentration profile shows two distinct phases; a phase where the interstitial H atoms form a local nano-hydride. The local hydride is surrounded by the second phase where the interstitial H atoms are dilute and form a lattice gas.

To understand the origin of this two phase regime, we can consider the thermodynamic stability of the hydride as a function of external pressure. At zero pressure and chemical potentials considered here (which correspond to a few ppm H bulk concentration) the formation of bulk hydrides is for many metals endothermic and therefore not observed. However, applying a positive hydrostatic (dilatational) stress expands the lattice and thus thermodynamically stabilizes the formation of the hydride. The tensile stress fields induced by the dislocation therefore cause regions in the solid where the formation of typically highly localized hydrides becomes thermodynamically possible. Theoretical work on local hydride formation around stress concentrators, such as dislocations [1,28] and cracks [34,35] have been reported earlier. These local hydrides are confined to the regions where tensile strain is induced, i.e., once formed they grow until their equilibrium size has been achieved. The equilibrium size can reach the order of a few nm, as shown in Fig. 3. If the chemical potential remains unchanged, further growth is not possible, i.e., the nano-sized features are stable against coarsening.

The formation of this local hydride lowers the free energy of the system and thus helps to stabilize the dislocation loop. Physically, the insertion of the hydrogen atoms in the tension side of the edge segments helps to mitigate the elastic energy increase due to the introduction of the dislocation loop. This attractive interaction between interstitial H atoms and dislocations results in an effective decrease in dislocation line energy and is an example of the "defactant" concept first introduced by Kirchheim [27].

Taking full advantage of the computational efficiency of the model, we calculated the equilibrium hydrogen concentration for dislocation radii ranging from 0 to $7b$ and bulk hydrogen concentrations ranging from 10^2 to 3×10^3 ppm at 300 K. Note that while atomistic simulations of nanoindentation have been performed [29], the strain rate in those calculations is too high for the hydrogen to diffuse to their equilibrium positions. The total number of excess hydrogen $\Delta N_{\text{H}} = \sum_i^{N^{\text{oct}}} (c_{\text{H}}^i - c_{\text{H}}^{\text{bulk}})$ with i running over all octahedral sites in the supercell is shown in Fig. 4. For a given radius r_{disl}, a critical concentration $c_{\text{H}}^{\text{bulk}}$ is required before a local hydride can form around the dislocation. This critical $c_{\text{H}}^{\text{bulk}}$ is higher for smaller r_{disl}. This is because smaller loops have weaker pressure fields due to the interaction with nearby segments. As the loop grows, the stress field approaches that of infinite straight dislocations. The critical concentration $c_{\text{H}}^{\text{bulk}}$ for nanohydride formation is considerably higher than that of straight edge dislocations [1], since

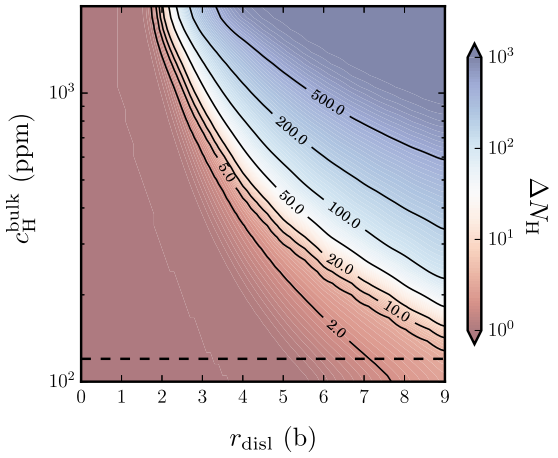

Fig. 4. Number of excess hydrogen atoms ΔN_{H} as a function of dislocation radius r_{disl} and bulk hydrogen concentration $c_{\text{H}}^{\text{bulk}}$ for $T = 300$ K. The contour plot shows the critical bulk H concentration necessary to form a local hydride around a dislocation loop with radius r_{disl}. After the hydride forms, ΔN_{H} increases dramatically with increasing r_{disl} and $c_{\text{H}}^{\text{bulk}}$. The dashed line is the critical concentration for an isolated partial dislocation, which corresponds to the case when $r_{\text{disl}} \to \infty$.

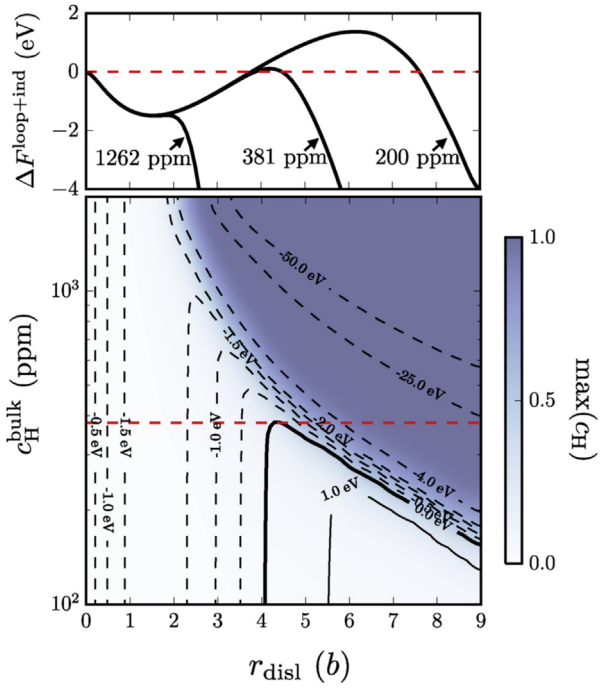

Fig. 5. *Above*: Formation energy to create a dislocation loop under the indenter $\Delta F^{\text{loop+ind}}$ (Eq. (8)) as a function of dislocation radius r_{disl} at $T = 300$ K and $\tau^{\text{ext}} = 4$ GPa at various bulk hydrogen concentrations $c_{\text{H}}^{\text{bulk}}$. The red dashed line indicates the free energy of the bulk system without a dislocation. *Below*: The line contours show the total energy change as a function of dislocation radius r_{disl} and bulk hydrogen concentration $c_{\text{H}}^{\text{bulk}}$ at $T = 300$ K. The external shear stress is $\tau^{\text{ext}} = 4$ GPa. The energy barrier becomes zero above a critical H concentration (shown by the red dashed line), indicating that HDN is spontaneous. The continuous blue contours correspond to the maximum hydrogen concentration in the system. If a local hydride forms in the system, this quantity approaches unity. (For interpretation of the references to colour in this figure legend, the reader is referred to the web version of this article.)

the two partials in a straight edge dislocation have the same direction. This leads to an increase in pressure field as the two partials are brought together. In contrast, the opposite segments in the dislocation loop have different line directions, leading to a decrease in pressure field if brought together (i.e., as $r_{\text{disl}} \to 0$).

Once the equilibrium hydrogen concentration has been calculated, the energy needed to create a dislocation loop as a function of bulk hydrogen concentration $c_{\text{H}}^{\text{bulk}}$ and temperature T can be straightforwardly calculated using Eqs. (4)–(8). A typical energy landscape is depicted in Fig. 5 for $\tau^{\text{ext}} = 4$ GPa. At low H concentrations $c_{\text{H}}^{\text{bulk}}$ (low μ_{H}), a dislocation loop growing from $r_{\text{disl}} = 0$ to $r_{\text{disl}} = \infty$ encounters a barrier. However, above some critical $c_{\text{H}}^{\text{bulk}}$ (or equivalently μ_{H}), the energy monotonically decreases with increasing dislocation radius r_{disl}, indicating that the HDN process above this concentration is no longer activated but is spontaneous.

The energy profile of the system (Fig. 5) shows a minimum at $r_{\text{disl}} = 1.5b$. However, preliminary molecular static simulations show no evidence that such small loops can be stabilized. This discrepancy is likely related to the fact that the model underestimates the dislocation core energy, since the model only takes the stable stacking fault energy γ_{sf} rather than the full gamma surface of the system. This error scales with the loop perimeter and increases with decreasing loop radius. As the ratio between loop area and length increases, the contribution to this error becomes smaller. To take this into account, we adopt the convention of assuming that the energy increases monotonically from $r_{\text{disl}} = 0$ up to the critical dislocation loop radius where the energy is maximum [25,26,33]. The energy barrier is therefore taken to be the maximum energy at any given $c_{\text{H}}^{\text{bulk}}$ and τ^{ext}.

The energy barriers are extracted from the energy landscapes as a function of bulk hydrogen concentration $c_{\text{H}}^{\text{bulk}}$ and external shear τ^{ext}. The critical dislocation radius at which these barriers can be found always coincides with the start of local hydride formation, indicated by the edge of the blue contour in Fig. 5. These barriers are presented in Fig. 6, showing that after a critical bulk hydrogen concentration of $c_{\text{H}}^{\text{bulk}} \approx 300$ ppm, the energy barrier of HDN is drastically reduced by the H solutes. When the barrier is 0, the HDN process is spontaneous. The zero contour line can therefore be taken as a prediction on when HDN can occur.

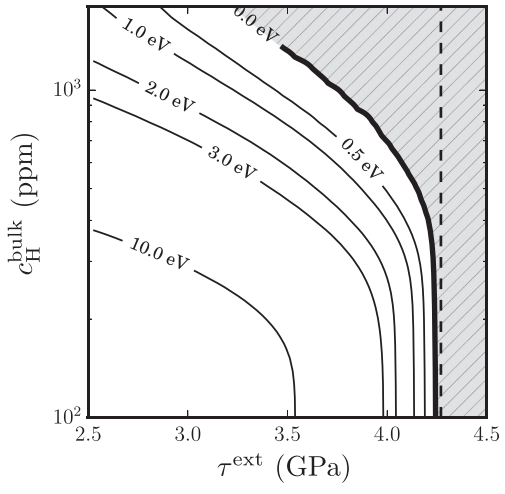

Fig. 6. The energy barrier to HDN as a function of dislocation radius r_{disl} and bulk hydrogen concentration $c_{\text{H}}^{\text{bulk}}$. The barrier drastically decreases after the critical $c_{\text{H}}^{\text{bulk}} \approx 300$ ppm is reached. The shaded area corresponds to the region wherein HDN is spontaneous (barrier-free). The dashed line is the critical shear stress required for HDN without hydrogen.

6.2. Effect of indenter pressure field

The analysis in the previous section assumes that the external stress field is purely deviatoric in nature. Conventional analysis of HDN assumes that the nucleation event would occur in the region of the material experiencing the largest deviatoric stress [25,26]. In nanoindentation experiments, however, the indenter also exerts a (compressive) pressure field that pushes hydrogen atoms underneath the indenter away. Since the presence of hydrogen affects the nucleation barrier to HDN, it is important to take the pressure field into account. This can be done by considering what the effective bulk hydrogen concentration is beneath the indenter,

$$c_{\text{H}}^{\text{bulk,eff}} = c_{\text{H}}^{\text{bulk}} \exp\left[\frac{p^{\text{ext}} \Delta v_m}{kT}\right], \tag{18}$$

where the external pressure field $p^{\text{ext}} = \frac{1}{3}\sigma_{kk}^{\text{ext}}$ is negative (compressive) in this case. Thus, $c_{\text{H}}^{\text{bulk,eff}}$ is always less than $c_{\text{H}}^{\text{bulk}}$ underneath the indenter. The previous analysis holds provided all instances of $c_{\text{H}}^{\text{bulk}}$ are replaced with $c_{\text{H}}^{\text{bulk,eff}}$.

To make this more concrete, we model the interaction with the indenter as a sphere forming a Hertzian contact with an elastic half-space. Other geometries might be considered, but this would not change the general conclusions of the analysis. The stress components due to the indenter in cylindrical coordinates are given by [2],

$$\frac{\sigma_r}{p_0} = \frac{\sigma_\theta}{p_0} = -(1+\nu)\left\{1 - \frac{z}{a}\tan^{-1}\frac{a}{z}\right\} + \frac{1}{2}\left(1 + \frac{z^2}{a^2}\right)^{-1}, \tag{19}$$

$$\frac{\sigma_z}{p_0} = -\left(1 + \frac{1+z^2}{a^2}\right)^{-1}, \tag{20}$$

where z is the coordinate perpendicular to the surface, a is the radius of the indenter (inset in Fig. 7(a)), and p_0 is the pressure at the center of the indenter on the surface. These principal stresses along with the principal shear stress $\tau = \frac{1}{2}|\sigma_z - \sigma_\theta|$ and pressure field $p = \frac{1}{3}(\sigma_r + \sigma_\theta + \sigma_z)$ are shown in Fig. 7(b). Typically, HDN is assumed to occur at the depth at which the principal shear stress is maximum (at $z/a = 0.45$) [25,26], since the pressure field does not affect the energetics of the dislocation nucleation. When mobile solutes are involved, this is no longer the case. The effective bulk hydrogen concentration as a function of depth is also shown in Fig. 7(a) for the case when $T = 300$ K. Due to the indenter pressure field, $c_{\text{H}}^{\text{bulk,eff}}$ at $z/a = 0.45$ is almost two orders of magnitude lower than $c_{\text{H}}^{\text{bulk}}$. The point at which HDN occurs can therefore no longer be assumed to occur where the principal shear stress is highest.

To assess the stability of the system against the nucleation of dislocation loops, Fig. 6 can be inverted to create a prediction of critical stress τ_c as a function of effective bulk hydrogen concentration $c_{\text{H}}^{\text{bulk,eff}}$. Since $c_{\text{H}}^{\text{bulk,eff}}$ increases with z, τ_c decreases as z increases. When τ_c is below the principle shear stress, HDN can occur. The above discussion allows us to make a direct comparison of the model's prediction with experiments made in Ref. [25]. The exact value of the bulk hydrogen concentration after charging in these electrostatic experiments is difficult to determine, but it is on the order of 1–2% [36]. After hydrogen charging, the pop-in force f_c dropped on average to approximately a half of its original value. Since the critical stress τ_c scales with the critical applied force $\sim f_c^{1/3}$, τ_c dropped by approximately 20% of its original value. The critical shear stress in the absence of hydrogen $\tau_c^{\text{H-free}}$ is predicted to be 4.25 GPa, in good agreement with 3.3 GPa obtained from experiments.

Fig. 7(c) shows τ_c and τ_{ext} as a function of normalized depth z/a at three different bulk hydrogen concentrations ($c_{\text{H}}^{\text{bulk}} = 0\%, 1\%$ and

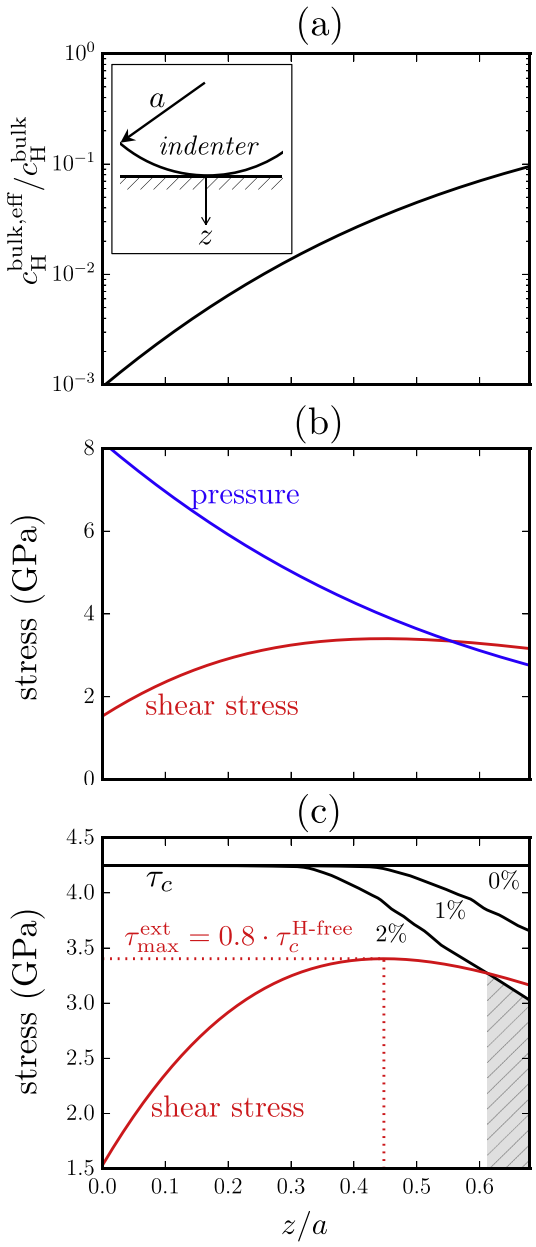

Fig. 7. (a) The effective bulk hydrogen concentration $c_H^{bulk,eff}$ normalized against the bulk hydrogen concentration c_H^{bulk} for $T = 300$ K as a function of depth z/a along the indenter axis. The maximum external shear stress is set at 80% of the critical shear stress for HDN without the presence of hydrogen τ_c^{H-free}. The inset in the right figure shows a schematic representation of the nanoindenter experiment. (b) The corresponding principal shear stress τ and the magnitude of the pressure field $|p|$ along z/a. (c) The critical shear stress for HDN τ_c and the external shear stress τ^{ext} as a function of normalized depth z/a for $c_H^{bulk} = 0\%, 1\%$ and 2% for $T = 300$ K. At the point of maximum external shear ($z/a = 0.45$), τ^{ext} is insufficient to initiate HDN for all cases. However, when $z/a > 0.61$, $\tau_c < \tau^{ext}$ for $c_H^{bulk} = 2\%$ (shown in the plot as the shaded region), indicating that HDN will spontaneously occur. HDN will not occur for the other concentrations.

2%) for the case when the maximum principal shear stress is 80% of the critical stress of the hydrogen-free nickel. At $z/a \sim 0.45$, where the principal shear stress is maximum, τ^{ext} is too low for HDN to occur for all cases. However, if we go to a larger ratio $z/a \approx 0.6$, the critical shear stress τ_c drops below τ^{ext} for the highest bulk concentration $c_H^{bulk} = 2\%$ considered here, indicating that HDN occurs spontaneously. The origin, as shown in Fig. 7(b), is that the principal shear stress falls slower than the pressure field exerted by the indenter. The prediction of the model is therefore consistent with previous nanoindentation experiments [25,26] but is able to reproduce and explain them, without the need to invoke hydrogen effects on shear modulus, dislocation core radius or stacking fault energy.

The analysis in this paper primarily deals with the energetics of HDN. However, the kinetics of the system is expected to play an important role since dislocation loop and the hydride depend on each other. A small subcritical loop is stabilized by the hydride, which in turn is stabilized by the dislocation's stress field. While a detailed analysis of the system's kinetics is beyond the scope of this work, we propose the following mechanism to explain how local hydrides might form around small dislocations. At a given stress below the critical value, it is possible to form small unstable dislocation loops at finite temperature. These loops would quickly collapse. Due to these fluctuations hydrogen is attracted to the dislocation loop until it collapses and would localize in regions that are energetically favorable. These in turn make the formation of the unstable dislocation loop a bit more energetically favorable, increasing the frequency of the fluctuation. This self-reinforcing process would continue until the critical loop radius is reached. Once the dislocation exceeds this radius, the dislocation can grow by incorporating additional hydrogen atoms and enhances plasticity.

The presented model may be regarded as a practical realization of the “defactant” concept introduced by Kirchheim [27], since both the solute-dislocation and hydrogen–hydrogen interaction are favorable and can be attributed to an effective decrease in the dislocation line energy. Here we have identified the origin of this interaction (both mechanical and chemical) and have quantified the effects given specific boundary conditions.

It should be noted that the indenter introduces significant stress concentrations in regions not directly underneath the indenter. In particular, large tensile stresses are expected at the surface close to the edge of the indenter [37]. However, modeling hydride formation at the surface requires a methodologically very different approach that is beyond the scope of the paper. Additionally, only a single dislocation loop has been considered in the analysis. If multiple dislocations are close enough together, then the formation of the local hydride phase might get affected. However, for this to happen, the spacing of the dislocation should be rather close (on the order of a few Burgers vector). As such, treatment of multiple dislocations in relation to hydride formation must be treated with care and will be explored in a future paper.

7. Conclusions

In this paper, we have extended our model for hydride formation around a straight edge dislocation [1] to describe the impact of local hydrides on the nucleation of dislocation loops. The derived multiscale model takes atomistic inputs, such as dislocation stacking fault energy, dislocation core structure and H–H interaction. In particular, H–H interaction plays a critical role in explaining the drop in pop-in force observed in experiments. The model faithfully predicts the spatially resolved equilibrium hydrogen concentration at finite temperature as a function of bulk hydrogen concentration (or equivalently, the hydrogen chemical potential μ_H). The exact distribution of the interstitial H in the vicinity of defects such as dislocation loops is critical to accurately describe the impact H has on plasticity but would be computationally challenging or unfeasible by molecular dynamics based atomistic approaches only.

The described concepts and formalisms regarding local phase transformation around stress concentrators can be extended to defects apart from dislocations. Examples are situations where

pressure fields induced by external loads activate mechanisms that without H are not operational. For instance, the pressure field in front of a crack tip may increase the local hydrogen concentration above a critical level to activate dislocation sources that would be inactive without the presence of hydrogen. Studying such systems will help elucidate the effect of hydrogen in failure mechanisms outside HDN. Employing the multiscale approach derived and outlined in the present study provides an efficient simulation tool to quantitatively describe such scenarios.

Acknowledgments

G.P.M.L is funded by a Postdoctoral Fellowship of the Alexander von Humboldt Foundation. The authors gratefully acknowledge the financial support of the Deutsche Forschungsgemeinschaft (DFG) within the Collaborative Research Center (SFB) 761 “Steel-*ab initio*” and by the European Research Council under the EU's 7th Framework Programme (FP7/2007–2013)/ERC Grant agreement 290998.

Appendix A. Stress field of a straight dislocation segment

The calculation of the stress field induced by a straight dislocation segment is summarized in this section. For a complete derivation of these expressions, readers are directed to Ref [33]. In the following equations, the coordinate system is chosen such that the dislocation segment lies along the z-axis. The components of the stress tensor due to the dislocation segment are then given by,

$$\frac{\sigma_{xx}}{\sigma_0} = b_x \frac{y}{R(R+\lambda)}\left[1+\frac{x^2}{R^2}+\frac{x^2}{R(R+\lambda)}\right] + b_y \frac{x}{R(R+\lambda)}\left[1-\frac{x^2}{R^2} - \frac{x^2}{R(R+\lambda)}\right], \tag{A.1}$$

$$\frac{\sigma_{yy}}{\sigma_0} = -b_x \frac{y}{R(R+\lambda)}\left[1-\frac{y^2}{R^2}+\frac{y^2}{R(R+\lambda)}\right] - b_y \frac{x}{R(R+\lambda)}\left[1+\frac{y^2}{R^2} + \frac{y^2}{R(R+\lambda)}\right], \tag{A.2}$$

$$\frac{\sigma_{zz}}{\sigma_0} = b_x\left[\frac{2\nu y}{R(R+\lambda)}+\frac{y\lambda}{R^3}\right] + b_y\left[-\frac{2\nu x}{R(R+\lambda)}-\frac{x\lambda}{R^3}\right], \tag{A.3}$$

$$\frac{\sigma_{xy}}{\sigma_0} = -b_x \frac{x}{R(R+\lambda)}\left[1-\frac{y^2}{R^2}-\frac{y^2}{R(R+\lambda)}\right] + b_y \frac{y}{R(R+\lambda)}\left[1-\frac{x^2}{R^2} - \frac{x^2}{R(R+\lambda)}\right], \tag{A.4}$$

$$\frac{\sigma_{xz}}{\sigma_0} = -b_x \frac{xy}{R^3} + b_y\left(-\frac{\nu}{R}+\frac{x^2}{R^3}\right) + b_z \frac{y(1-\nu)}{R(R+\lambda)}, \tag{A.5}$$

$$\frac{\sigma_{yz}}{\sigma_0} = b_x\left(\frac{\nu}{R}-\frac{y^2}{R^3}\right) + b_y \frac{xy}{R^3} - b_z \frac{x(1-\nu)}{R(R+\lambda)}, \tag{A.6}$$

where $R=\sqrt{x^2+y^2+(z-z')^2}$, $\sigma_0=\mu/4\pi(1-\nu)$ and $\lambda=z'-z$.

References

[1] G.P.M. Leyson, B. Grabowski, J. Neugebauer, Multiscale description of dislocation induced nano-hydrides, Acta Mater. 89 (2015) 50–59.
[2] W. Johnson, On some remarkable changes produced in iron and steel by the action of hydrogen and acids, Proc. R. Soc. Lond. 23 (1874) 168–179.
[3] G.M. Bond, I.M. Robertson, H.K. Birnbaum, The influence of hydrogen on deformation and fracture processes in high-strength aluminum alloys, Acta Metall. 35 (9) (1987) 2289–2296.
[4] G.M. Bond, I.M. Robertson, H.K. Birnbaum, Effects of hydrogen on deformation and fracture processes in high-purity aluminum, Acta Metall. 36 (8) (1988) 2193–2197.
[5] D.H. Lassila, H.K. Birnbaum, The effect of diffusive hydrogen segregation on fracture of polycrystalline nickel, Acta Metall. 34 (7) (1986) 1237–1243.
[6] D.H. Lassila, H.K. Birnbaum, Intergranular fracture of nickel: the effect of hydrogen-sulfur co-segregation, Acta Metall. 35 (7) (1987) 1815–1822.
[7] D.H. Lassila, H.K. Birnbaum, The effect of diffusive segregation on the fracture of hydrogen charged nickel, Acta Metall. 36 (10) (1988) 2821–2825.
[8] G.M. Bond, I.M. Robertson, H.K. Birnbaum, On the mechanisms of hydrogen embrittlement of Ni_3 Al alloys, Acta Metall. 37 (9) (1989) 1407–1413.
[9] S. Bechtle, M. Kumar, B.P. Somerday, M.E. Launey, R.O. Richie, Grain-boundary engineering markedly reduces susceptibility to intergranular hydrogen embrittlement in metalling materials, Acta Mater. 57 (2009), 2148–4157.
[10] D.S. Shih, I.M. Robertson, H.K. Birnbaum, Hydrogen embrittlement of α titanium: *in situ* TEM studies, Acta Metall. 36 (1) (1988) 111–124.
[11] T. Tabata, H.K. Birnbaum, Direct observation of the effect of hydrogen on the behavior of dislocations in iron, Scr. Metall. 17 (1983) 947–950.
[12] T. Tabata, H.K. Birnbaum, Direct observation of hydrogen enhanced crack propagation in iron, Scr. Metall. 18 (1984) 231–326.
[13] R.A. Oriani, P.H. Josephic, Equilibrium aspects of hydrogen-induced cracking of steels, Acta Metall. 22 (1974) 1065–1074.
[14] P. Sofronis, I.M. Robertson, Transmission electron microscopy observations and micromechanical/continuum models for the effect of hydrogen on the mechanical behaviour of metals, Phil. Mag. 82 (17–18) (2002) 3405–3413.
[15] S. Gahr, M.L. Grossbeck, H.K. Birnbaum, Hydrogen embrittlement of Nb I. macroscopic behavior at low temperatures, Acta Metall. 25 (2) (1977) 125–134.
[16] H. Vehoff, W. Rothe, Gaseous hydrogen embrittlement in FeSi- and Ni-single crystals, Acta Metall. 31 (11) (1983) 1781–1793.
[17] W.W. Gerberich, R.A. Oriani, M.J. Lji, X. Chen, T. Foecke, The necessity of both plasticity and brittleness in the fracture thresholds of iron, Phil Mag. 63 (2) (1991) 363–376.
[18] S. Serebrinskya, E.A. Carter, M. Ortiz, A quantum-mechanically informed continuum model of hydrogen embrittlement, J. Mech. Phys. Solids 52 (2004) 2403–2430.
[19] C.D. Beachem, A new model for hydrogen-assisted cracking hydrogen embrittlement, Metall. Trans. 3 (1972) 437–451.
[20] I.M. Robertson, H.K. Birnbaum, An HVEM study of hydrogen effects on the deformation and fracture of nickel, Scr. Metall. 34 (4) (1986), 535–366.
[21] P.J. Ferreira, I.M. Robertson, H.K. Birnbaum, Hydrogen effects on the interaction between dislocations, Acta Mater 46 (5) (1998) 1749–1757.
[22] P.J. Ferreira, I.M. Robertson, H.K. Birnbaum, Hydrogen effects on the character of dislocations in high-purity aluminum, Acta Mater 47 (10) (1999) 2991–2998.
[23] S.M. Myers, M.I. Baskes, H.K. Birnbaum, J.W. Corbett, G.G. DeLeo, S.K. Estreicher, E.E. Haller, P. Jena, N.M. Johnson, R. Kirchheim, S.J. Pearton, M.J. Stavola, Hydrogen interactions with defects in crystalline solids, Rev. Mod. Phys. 64 (2) (1992) 559–617.
[24] H.K. Birnbaum, P. Sofronis, Hydrogen-enhanced local plasticity–a mechanism for hydrogen related fracture, Mater. Sci. Eng. A 176 (1994) 191–202.
[25] A. Barnoush, H. Vehoff, Recent developments in the study of hydrogen embrittlement–hydrogen effect on dislocation nucleation, Acta. Mater. 58 (2010) 5274–5285.
[26] A. Barnoush, C. Bies, H. Vehoff, In situ electrochemical nanoindentation of FeAl(001) single crystal: hydrogen effect on dislocation nucleation, J. Mater. Res. 58 (2009) 1105–1113.
[27] R. Kirchheim, Revisiting hydrogen embrittlement models and hydrogen-induced homogenous nucleation of dislocations, Scr. Mater. 62 (2010) 67–70.
[28] J. von Pezold, L. Lymperakis, J. Neugebauer, Hydrogen-enhanced local plasticity at dilute bulk H concentrations: the role of H-H interactions and the formation of local hydrides, Acta Mater 59 (2011) 2969–2980.
[29] M. Wen, L. Zhang, B. An, S. Fukuyama, K. Yokogawa, Hydrogen-enhanced dislocation activity and vacancy formation during nano-indentation in nickel, Phys. Rev. B 80 (2009) 094113.
[30] J.E. Angelo, N.R. Moody, M.I. Baskes, Trapping of hydrogen to lattice-defects in nickel, Model Simul. Mater. Sci. Eng. 3 (3) (1995) 289–307.
[31] L.M. Brown, Wulff's theorem and certain green's functions in dislocation theory, Can. J. Phys. 45 (1967) 893–901.
[32] L.M. Brown, M.S. S, M. Ipohorski, The shape of frank loops studied by high-voltage microscopy, Philos. Mag. 24 (1971) 1495–1499.
[33] J.P. Hirth, J. Lothe, Theory of Dislocations, second ed., John Wiley & Sons, Inc., 1982.
[34] J. Song, W.A. Curtin, A nanoscale mechanism of hydrogen embrittlement in metals, Acta. Mater. 59 (2011) 1557–1569.
[35] J. Song, W.A. Curtin, Atomic mechanism and prediction of hydrogen embrittlement in iron, Nat. Mater. 10 (2012) 1–7.
[36] A. Barnoush, Personal communciations.
[37] C. Atkinson, J.M. Martnez-Esnaola, M.R. Elizalde, Contact mechanics: a review and some applications, Mater. Sci. Technol. 28 (2012) 1079–1091.